Available online at www.sciencedirect.com
SCIENCE DIRECT®
International Journal of Heat and Mass Transfer 47 (2004) 5713–5724
International Journal of HEAT and MASS TRANSFER
www.elsevier.com/locate/ijhmt

Spray cooling characteristics of water and R-134a. Part II: transient cooling

Shou-Shing Hsieh *, Tsung-Cheng Fan, Huang-Hsui Tsai

Department of Mechanical and Electro-Mechanical Engineering, National Sun Yat-Sen University, Kaohsiung, Taiwan 80424, Republic of China

Received 1 December 2003; received in revised form 16 June 2004
Available online 16 September 2004

Abstract

Spray cooling of a hot surface was investigated in the second of two papers to determine the effect of mass flux, Weber number, and degree of subcooling on two different working fluids such as pure water and R-134a. Full cone circular sprays were used to cool a circular surface of diameter 80 mm with an initial temperature about 250/70 °C for pure water/R-134a, respectively. Both the transient liquid crystal technique (only for R-134a) and thermocouple wire temperature measurements were conducted. Cooling curves were obtained in a wide range of the above-mentioned parameters.

1. Introduction

There has been an increased demand for new technique capable of removing high heat fluxes and such demands will continue to increase in the future. Among these techniques, spray cooling is one of the most notable methods to remove high heat fluxes. Applications exist in a wide range of industrial processes including rapid cooling and quenching in metal foundries, emergency of core cooling systems, cooling of microelectronics and ice chiller in air-conditioning systems. Most relevant studies [1,2] have been examined in Part I of this study. However, there seems only few papers to deal with the transient spray cooling. Most recently, Cui et al. [3] experimentally studied the effect of dissolving salts in water sprays used for quenching a hot surface. Both transient temperature distribution and surface heat flux were calculated. It is found that some dissolving salts would increase nucleate boiling heat transfer, but had little effect on transition boiling. Bernardin et al. [4] recorded the impact behavior of water droplets on a hot aluminum surface using a high speed photographic technique. It was found that droplet velocity and surface temperature were two important parameters governing the impact behavior and ensuring heat transfer.

Part I of this study addressed steady state boiling experiments during the spray cooling. This study, Part II, presents the results of liquid sprays of both water and R-134a during transient cooling. Prior to spray cooling, the test surface was initially heated to a constant temperature of 240 °C and 60 °C for water and R-134a, respectively. Cooling curves were obtained for different spray mass flux, Weber number, degree of superheat and degree of subcooling. The transient experiments in this work would provide necessary information and heat transfer characteristics through the film,

* Corresponding author. Tel.: +886 7 5252000x4215; fax: +886 7 5254215.
E-mail address: sshsieh@mail.nsysu.edu.tw (S.-S. Hsieh).

0017-9310/$ - see front matter © 2004 Elsevier Ltd. All rights reserved.
doi:10.1016/j.ijheatmasstransfer.2004.07.023

Nomenclature

A	area of test surface, m^2
C_p	specific heat for spray liquid, kJ/kg °C
d	droplet mass median diameter, m
d_j	nozzle diameter, m
d_{32}	Sauter mean diameter (SMD), m
h	TLC detailed/or an average (for thermocouple measurements) heat transfer coefficient, W/m^2 °C
$\bar{h}$	TLC average heat transfer coefficient, W/m^2 °C
h_{fg}	enthalpy of evaporation, J/kg
$\dot{m}$	spray mass flux, kg/m^2s
k	thermal conductivity, W/m °C
q	heat flux, W/m^2
q_{CHF}	critical heat flux, W/m^2
$q_{max/min}$	maximum/minimum heat flux, W/m^2
u_0	mean spray impingement velocity, m/s
We	spray Weber number, $\rho_l u_0^2 d_{32}/\sigma$
x	distance from nozzle to test surface

Greek symbols

ΔT_{sat}	wall superheat, °C
ΔT_{sub}	degree of subcooling, °C
ρ	density of liquid, kg/m^3
σ	surface tension of spray liquid, N/m

transition and boiling regimes. The emphasis of this work is primary transient experimental and the objectives were to

(1) collect a certain amount of data for R-134a and pure water in transient spray cooling,
(2) investigate the transient spray cooling characteristics under relevant parameters and variables,
(3) obtain a detailed transient heat transfer data using the transient liquid crystal (TLC) technique.

2. Experimental

For heat transfer measurements, TLC (only for R-134a) and traditional thermocouple measurements were both conducted. However, due to the transient nature, the test surface was made from a very thin (0.5 μm) Pt sputtered circular surface as stated in Part I of this paper to ensure isothermal conditions throughout the disk at every instant during the experiments.

2.1. Heater design and temperature measurements

In addition to the heater design mentioned in Part I, the disk surface was also measured by three type K thermocouples with a diameter of 0.3 mm bonded to the disk underside in sequential manner along the center line as shown in Fig. 1. High thermal conductivity paste (alumina/silica, $k = 8.4$ W/m °C) was applied to the thermocouples to warrant good contact between the copper substrate and the thermocouple bead. Heat conduction within the copper disk was high enough to give an almost uniform temperature profile along its centerline ($\leqslant 1$ °C). The transient temperature data were recorded every 20 ms until the disk temperature fell below a certain temperature for pure water and R134a. It was possible to estimate the heat flux either using Fourier's law of heat conduction [5] or the sequential function specification method to solve one-dimensional inverse problem [3]. Both methods were used and compared for double check. The present surface heat flux calculation was found to within ±12%. The transient experiments using the present heater designed can provide the heat transfer characteristics throughout the film, transition, nucleate, and forced convection and evaporation regions. The critical as well as minimum heat flux (CHF and MHF) can also be obtained. Relevant uncertainty estimates were listed in Table 1.

2.2. Transient liquid crystal measurements

The experimental apparatus includes a flow circuit, thermochromatic liquid crystal imaging test section, and instruments, which is schematically shown in Fig. 2. A scanning electron microscope (SEM) image of the Pt surface is depicted in Fig. 3(a) and (b). With different magnification, the surface condition seen is different even under a same power applied (=10.0 kV). The crack with island-like porous nano/micro structure was clearly noted for ×100,000 photograph; while for ×60,000 more larger islands without a crack were found. A Panasonic CCD camera (model: AVC597NIF36) with a light source directly facing the nozzle exit, and mounted on a vertical stationary post was used with a maximum speed of 3 frames/s in NTSC format to record the color change of the liquid crystal coating as the liquid spray impinged onto the test surface.

The time of color change of the liquid crystal driving a transient test is measured by a Panasonic 1/4″ color CCD image senor and a computer vision system. The test surface is airsprayed with black background paints first and then liquid crystal (Hallcrest, BM/R18C5W/

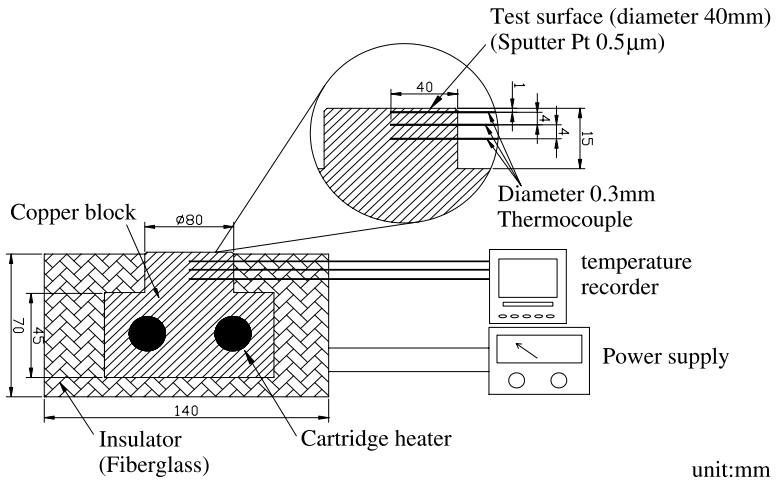

Fig. 1. Heater design and configuration with thermocouple measurement position.

Table 1
Uncertainties of relevant parameters/variables

Parameters/variables	Uncertainties	
Radius of test surface, r	±0.63%	
Heat surface area, A	±0.88%	
Wall temperature, T_w	R-134a	±0.16%
	Water	±0.45%
ΔT	R-134a	±0.48%
	Water	±0.51%
Thermocouple distance, Δx	±12.5%	
Heat flux, q	R-134a	±12.9%
	Water	±12.9%
Heat transfer coefficient, h	R-134a	±13.1%
	Water	±13.2%
Color change time (TLC), t	±4.2%	
Main stream temperature, T_∞	±3.6%	
Heat transfer coefficient (TLC)	±5.5%	

C17-10) of thickness of the order of 0.2 μm. Careful attention was paid to avoid influences due to the characteristic roughness of the TLC surface and black paint on the results. Meanwhile, thermophysical properties effect of the TLC were kept minimum and the uncertainty was estimated $< \pm 3\%$. Besides, a CCD camera, a frame grabber interface associated with Pentium III PC was used to analyze the color changes using a commercial image processing software (LCIA, Taiwan Pitot Co.) The image processing system maps the test section into 512×492 pixels (NTSC) locations and monitors each location individually for color change. Since the reflected light from liquid crystal is dependent on the spectral intensity of the incident light and contains a peak value whose wavelength inversely depends on the temperature [6], the test chamber is shielded from room light and room air currents using thick black felt curtain covered in such way that the test surface only receives incident light emitted from the light source mounted inside the CCD.

The light source used for this series of tests is a standard 60 mm Taiwan Concept cool white fluorescent lamp (13W NB4210-60 mm). The typical cool white fluorescent has a color temperature of 4100 K and a spectral

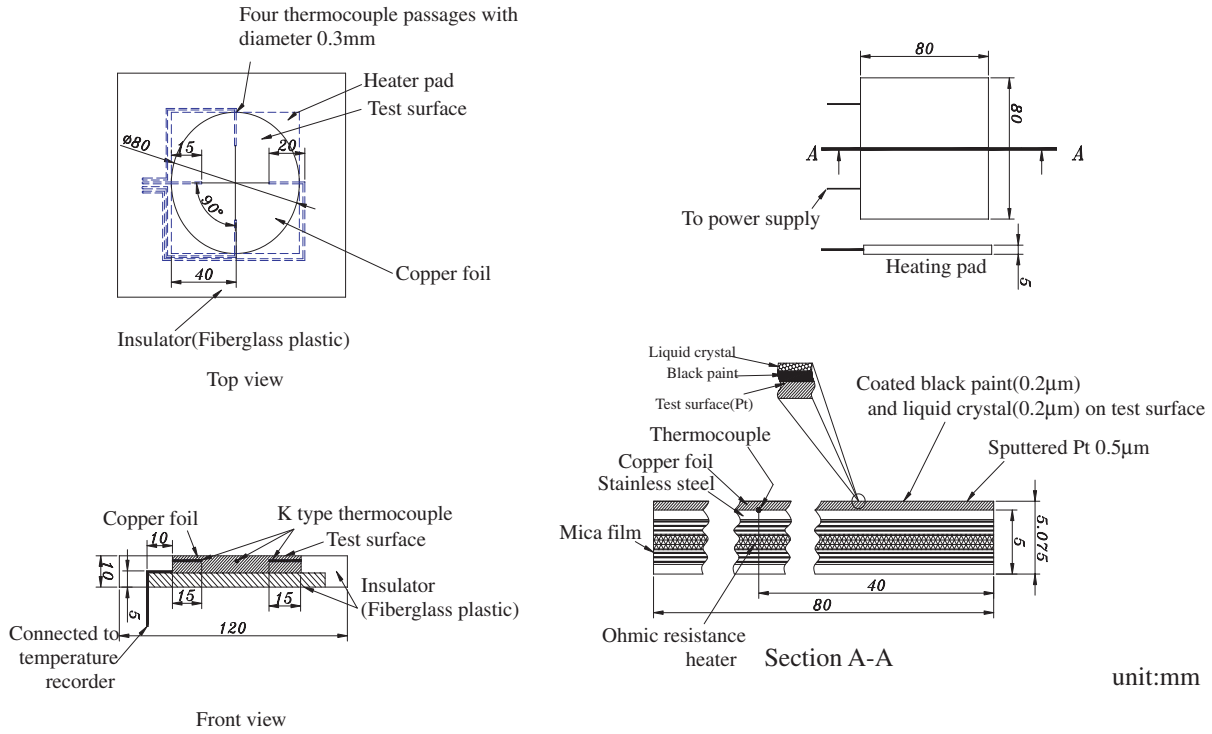

Fig. 2. Heating plate configuration for TLC measurement.

distribution that is high in the yellow–green range. In order to reduce the UV radiation damage to transient liquid crystal, a spectrum EB-74 UV sleeve filter was used to obtain 100% UV blockage. A lens with an extended view angle of 70° was implement with the present CCD camera to minimize angle effects and to achieve uniform illumination intensity throughout the domain measured.

2.3. Analysis of liquid crystal thermography and experimental procedure

The local heat transfer coefficient over the target wall can be obtained by assuming one-dimensional transient conduction over a semi-infinite solid wall with the initial and boundary conditions on the liquid crystal coated surfaces are

$$\begin{aligned} &\rho_s C_{ps}\frac{\partial T}{\partial t} = k\frac{\partial^2 T}{\partial z^2} \\ &T = T_i \quad \text{at } t = 0 \text{ and } z \geqslant 0 \\ &k\frac{\partial T}{\partial z} = h(T_w - T_\infty) \quad \text{at } z = 0 \\ &T = T_i \quad \text{as } t \to \infty \end{aligned} \tag{1}$$

This gives the dimensionless wall temperature response as follows:

$$\frac{T_w - T_i}{T_\infty - T_i} = 1 - \exp\left(\frac{h^2\alpha t}{k^2}\right)\operatorname{erfc}\left(\frac{h\sqrt{\alpha t}}{k}\right) \tag{2}$$

Once, for instance, T_i (up to 32 °C), T_∞ (~14 °C), and the corresponding time (t) required to change the coated-surface color to green are known, the heat transfer coefficient h can be estimated from Eq. (2). The green color of the liquid crystal shows the largest light intensity, which is a reference point that conventionally uses. Noting that in Eq. (2), the original T_∞ is a constant. However, in the present study, T_∞ is time-dependent and increases as the time (t) increases which can be simulated as a series of step functions. Applying the Duhamel's superposition principle, Eq. (2) can be rewritten in the following:

$$T_w - T_i = \sum_{j=1}^{N}\left[1 - \exp\left(\frac{h^2\alpha(t-\tau_j)}{k^2}\right) \times \operatorname{erfc}\left(\frac{h(\sqrt{\alpha(t-\tau_j)})}{k}\right)\right](\Delta T_\infty) \tag{3}$$

where ΔT_∞ and τ_j are the temperature and time step changes from the recorder readout. Since the time duration is too short to make the heat transport to the plexiglass plate, this assesses the assumption of the semi-infinite solid wall as stated before.

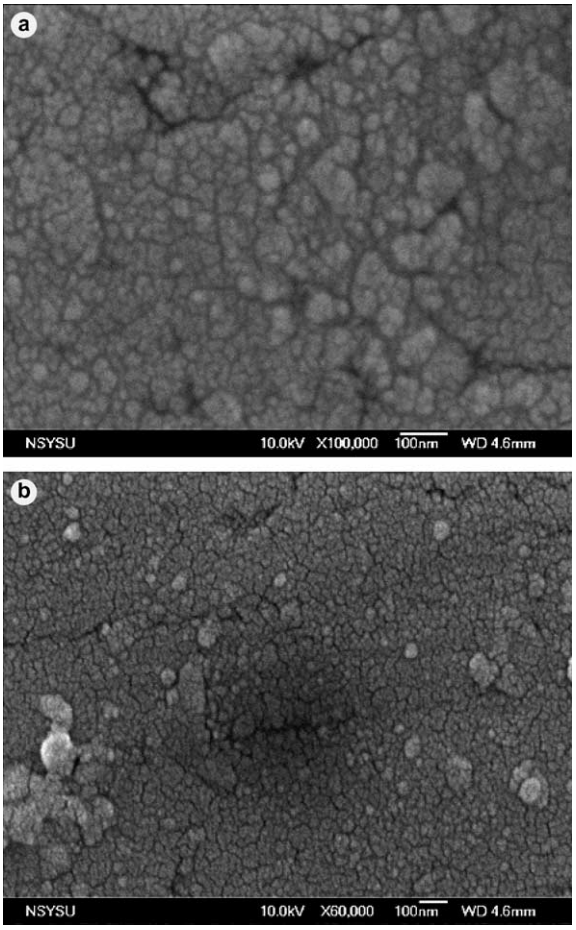

Fig. 3. SEM photographs (×100,000 and ×60,000) of the Pt test surface.

During the tests, the liquid crystal initially is colorless at chamber temperature (about 32 °C) and then it changes to blue, green, red, and finally colorless again. The total temperature change of the liquid crystal is about 5 °C (23–18 °C) for the color changes. The time for the color change is about 12–15 s for the cases under study. The color change temperatures to blue, green and red are 22.6, 18.2, and 17.6 °C, respectively. The accuracy of the time period for a color change is within ±4.2% and the chamber temperature has an error of about ±3.6% Once the test section including target surface coated with liquid crystals has been setup, tests were conducted by suddenly exposing the liquid to the test surface. This results in a color change of the surface coating. Before each test, the test section was kept at the chamber ambient temperature (~32 °C). Positioned with an angle 15° to the normal axis over the target walls is a three-chip Sony CCD camera. This angle effect was examined and found negligible under the present TLC space resolution. Each image is captured as a three-dimensioned matrix of red, green, and blue values. The image size is $320 \times 240 \times 3$ (≅0.22 MB). Image processing begins with a captured image for the entire target walls which is 320×240 pixels. During the experiments, the image processing system records the time for the color change to green for the entire surface. Finally, the time and temperature are logged in a computer program to obtain the local heat transfer coefficient.

Spray parameters used are the same in Part I of this paper. The operating and test conditions can be also found in Part I of the paper. The test surface was cleaned prior to each measurement by washing it first with acetone and, then cleaning it with distilled water. It was heated to 70 °C (R-134a) and 250 °C (water) by regulating the power to the heaters. Then the liquid supply pump was switched on. Once the nozzle pressure reached a steady value, the power to the heaters was turned off and remove the plastic plate shield simultaneously to allow liquid spray from the nozzle to quench the test surface. It usually takes $0 \sim 470$ s, depending on spray parameters, to cool the test surface from 70 °C (R-134a)/250 °C (water) to 15 °C (R-134a)/80 °C (water). Temperatures measured by thermocouples were continuously recorded by a data acquisition system. TLC measurements were simultaneously conducted. In addition, boiling phenomena photographs at selected conditions were taken as stated earlier.

3. Results and discussion

As one may know, the surface temperature of the test surface is the most important parameter in quenching and is used to define the four distinct heat transfer regimes of the boiling curve: (1) film boiling (2) transition boiling, (3) nucleate boiling, and (4) single phase liquid cooling. The boiling curve has found in most boiling studies as part I of this paper did. While, for quenching studies, the temperature as well as surface heat flux vs. time/or cooling curve shown in Fig. 4 are frequently encountered. In Fig. 4, the common encountered film boiling regime persists from elevated surface temperature down to a lower limit used to be referred to minimum heat flux (MHF) or Leidenfrost point (indicated by arrows) below which the transition boiling occurs. As the surface temperature decreases from Leidenfrost in the transition boiling regime (e.g. $25\,^{\circ}\mathrm{C} < T_w < 50\,^{\circ}\mathrm{C}$, at $We = 152$), the heat transfer rate increases as more efficient surface wetting and boiling occur. At the lower temperature boundary of the transition boiling regime, where the entire surface becomes available for wetting and heat transfer rate reaches a maximum (so called CHF). This maximum heat flux can be seen from the steepest portion (or inflection point indicated by arrows) of the cooling curves in Fig. 4. Below CHF (e.g. $q'' \approx 2.4 \times 10^4\,\mathrm{W/m^2}$ at $We = 152$ and $\Delta T_{sub} = 4\,^{\circ}\mathrm{C}$),

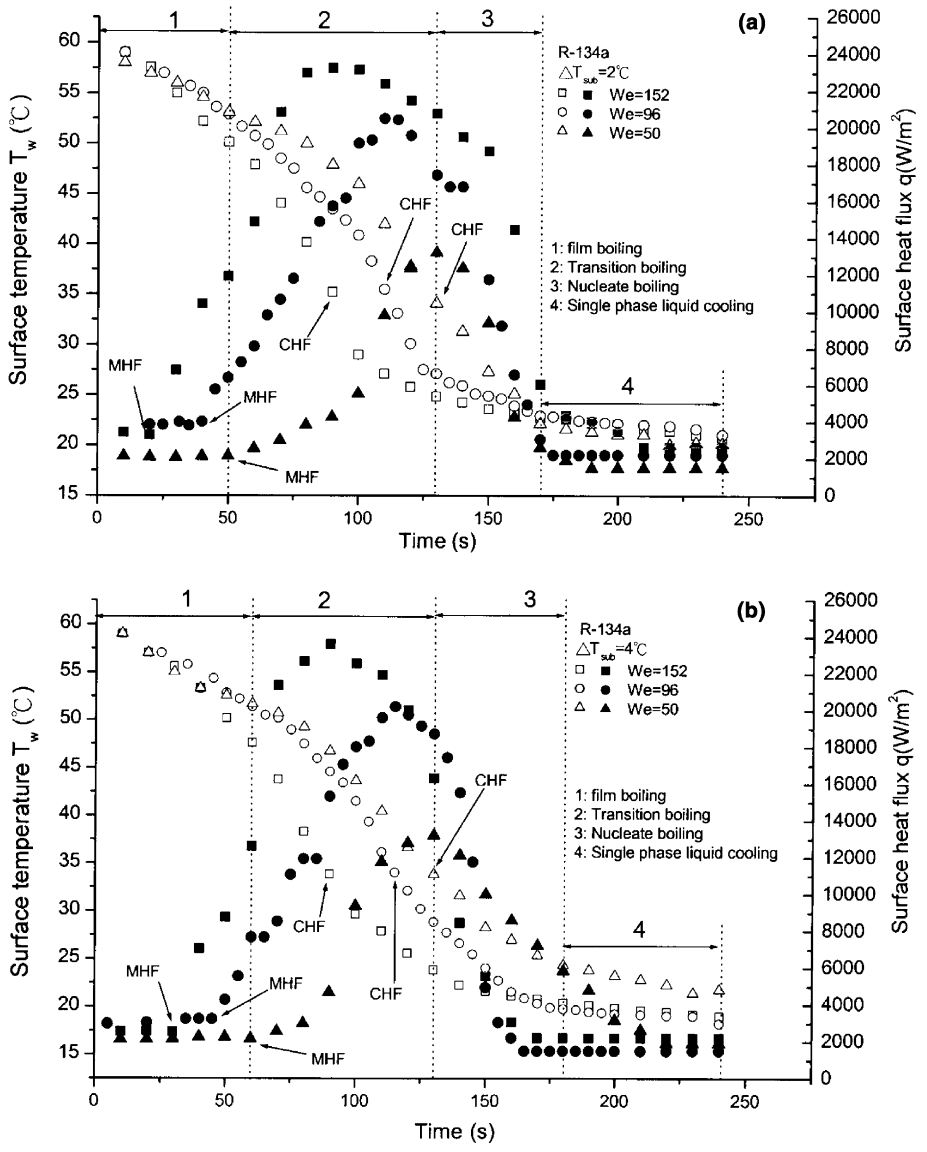

Fig. 4. Cooling curves for R-134a (solid symbols: surface heat flux, open symbols: surface temperature).

the heat transfer rate in nucleate boiling (e.g. $20\,^{\circ}\mathrm{C} < T_w < 25\,^{\circ}\mathrm{C}$ at $We = 152$) decreases with decreasing surface temperature. The lower temperature boundary of the nucleate boiling is determined by the minimum wall superheat (e.g. $T_w \leqslant 20\,^{\circ}\mathrm{C}$ at $We = 152$) required to sustain vapor bubble nucleation and growth within the impinging droplets. The film evaporation/or single phase forced convection would exist below the boundary (e.g. $q'' \leqslant 2 \times 10^3\,\mathrm{W/m^2}$ at $We = 152$ and $\Delta T_{sub} = 4\,^{\circ}\mathrm{C}$).

Based on the above physical heat transfer mechanism, the present results shown in Fig. 4(a) and (b) for two subcoolings are thus analyzed. For both cases with R-134a, elapsed time is about 240 s with different *We*. Generally, the Weber number effect can be clearly noted at $\Delta T_{sub} = 2\,^{\circ}\mathrm{C}$. Although, for $\Delta T_{sub} = 4\,^{\circ}\mathrm{C}$, the effect seems still significant, the ranges influenced became less as compared to that for $\Delta T_{sub} = 2\,^{\circ}\mathrm{C}$.

Also shown in Fig. 4(a) and (b) are the surface (wall) heat flux distribution. For both cases the maximum surface heat flux occurred at about $t = 100$–125 s. The surface heat flux increases as We increases as one would expect. Within uncertainty in heat flux, there seems no significant difference for these two different subcoolings.

Fig. 5(a) and (b) show the corresponding boiling curves of Fig. 4 at $\Delta T_{sub} = 2$ and $4\,^{\circ}\mathrm{C}$, respectively. It

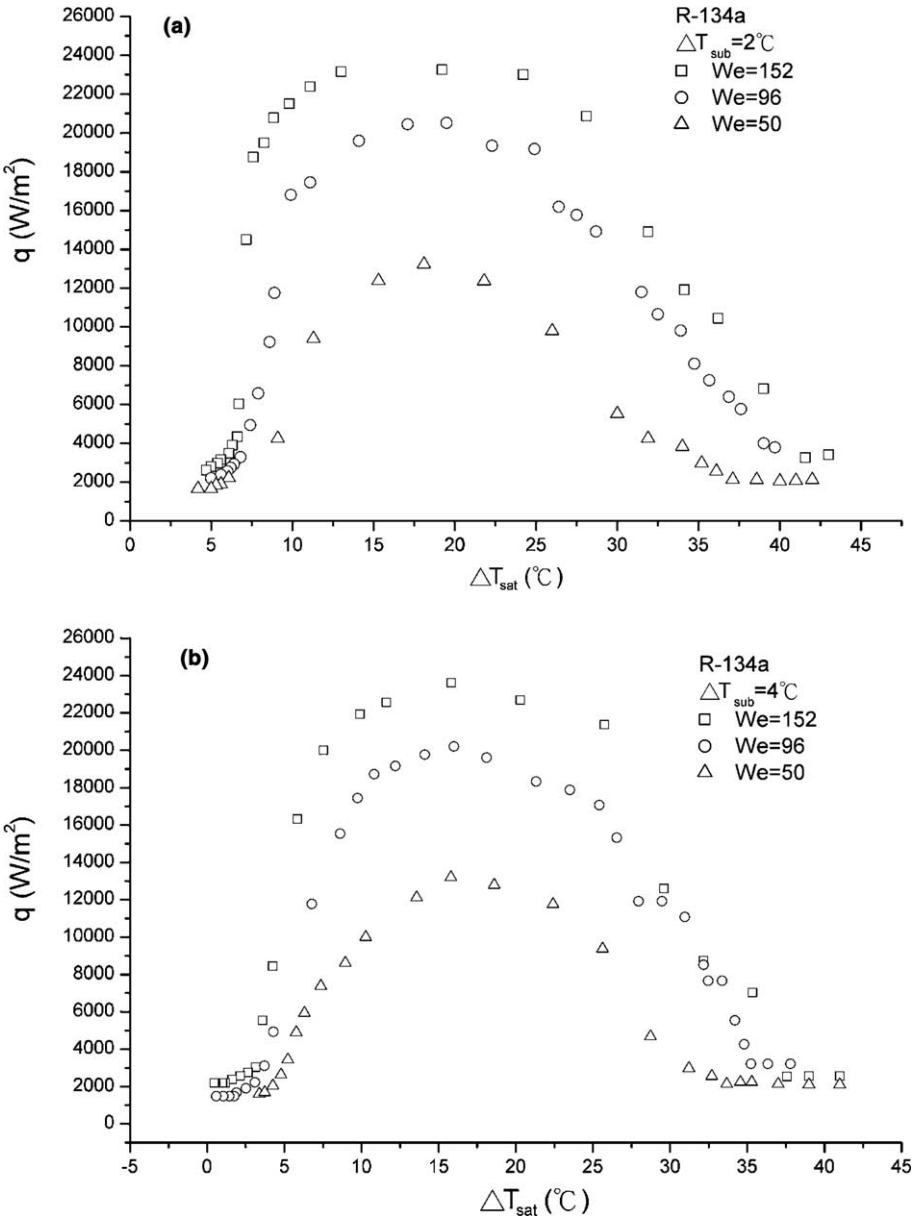

Fig. 5. The corresponding boiling curves (R-134a).

is clearly seen that the above- stated four regimes exist for both $\Delta T_{sub} = 2\,^{\circ}C$ and $4\,^{\circ}C$ subcoolings. The effect of subcoolings on heat flux seems not noted due to a small difference between these two subcoolings. However, the effect on ΔT_{sat} as compared both Fig. 5(a) and (b) can be stilled noted. In addition, the effect of Weber number is clearly noted again. The phenomenon associated was observed by Yoshida et al. [2] where they found, when $We \geqslant 80$, each droplet having impinged upon the heater surface was crashed to disintegrate into small fragments; while when $We < 80$, each droplet was subject to a deformation but it soon restored its spherical shape and then rebounded from the test surface. Generally, the boundaries to the boiling regimes, MHF and CHF, are nearly independent of spray *We*. However, the droplet dynamics and corresponding heat transfer mechanisms are different. In fact, the impact characteristics in each regime, such as droplet breakup, spreading rate, and film stability are strongly dependent on spray *We*. These behavior have been also reported in Bernardin et al. [4]. Based on Bernardin et al. [4], the present spray *We* tested belongs to

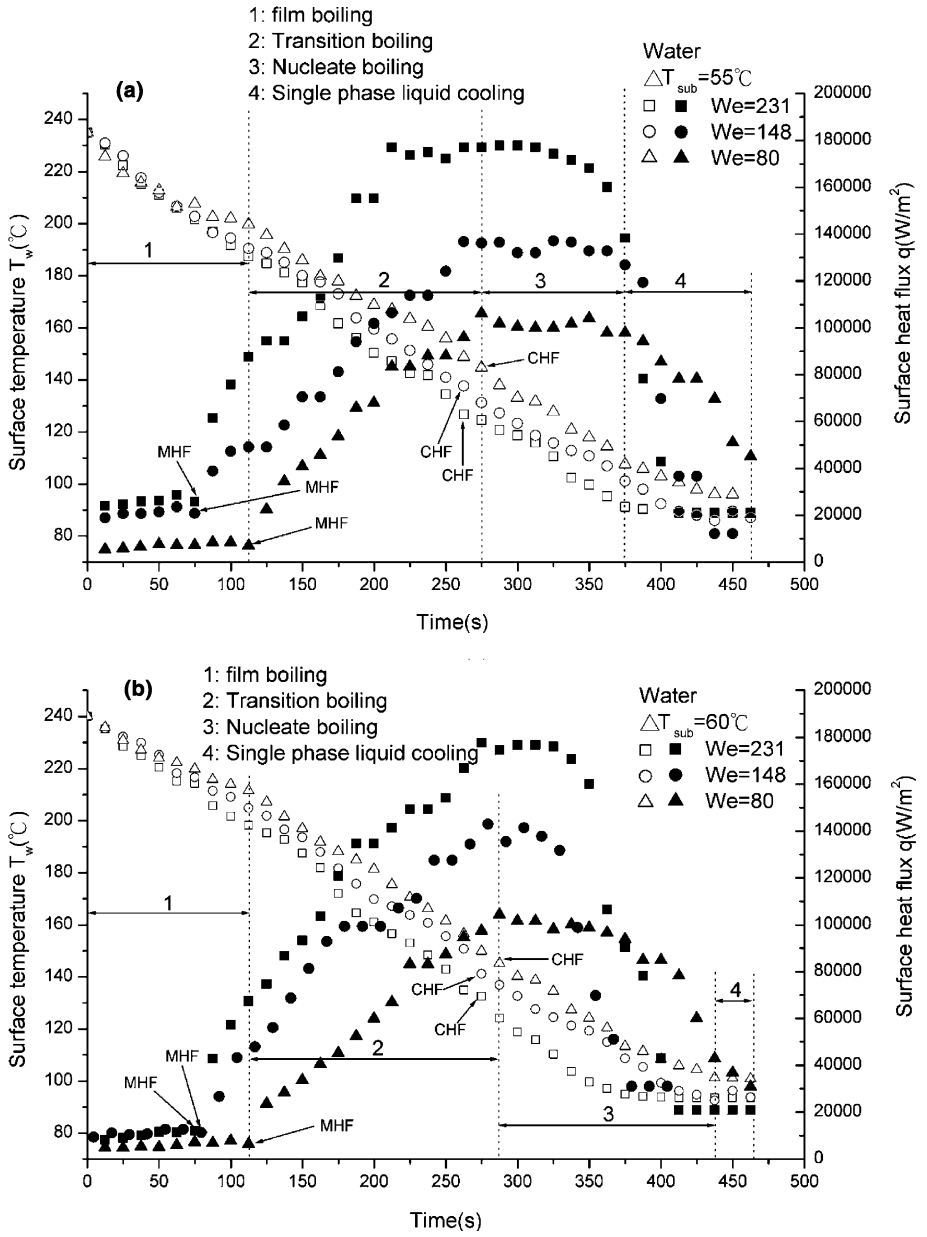

Fig. 6. Cooling curves for water (solid symbols: surface heat flux, open symbols: surface temperature).

intermediate ($We \leqslant 96$) and high Weber numbers ($We > 96$).

Fig. 6(a) and (b) show, on the other hand, pure water cooling performance at $\Delta T_{sub} = 55\,^{\circ}C$ and $60\,^{\circ}C$ with three different We. The corresponding boiling curves (q_{CHF} and q_{min} shown by arrows) were illustrated in Fig. 7(a) and (b), respectively. Generally, the above-mentioned four distinct heat transfer regime were again found as the same to R-134a cases. However, the starting temperature at which the transient experiment starts for pure water seems much higher, about $240\,^{\circ}C$ and it takes a relatively longer time, about 470 s for completion of a cooling process. Three Weber numbers were used for water and all are higher than those used for R-134a. In addition, the surface heat flux seems as expected much higher as compared to those of R-134a. For instance, the present cooling characteristics results in Fig. 7 for $We = 80$ has the maximum $q \cong 1.0 \times 10^5\,W/m^2$ at $\Delta T_{sat} \cong 30\,^{\circ}C$, while, for R-134a, at $We = 96$ the maximum $q \cong 1.2 \times 10^4\,W/m^2$. This is

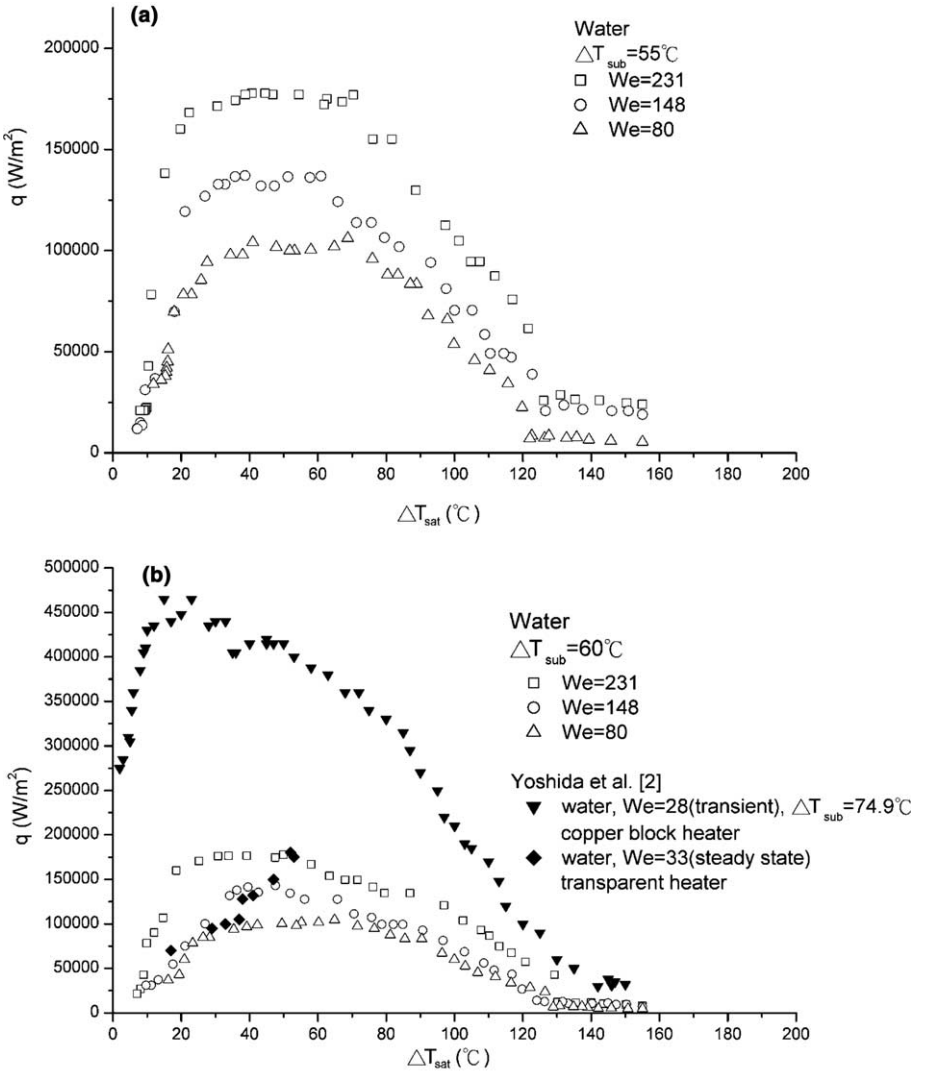

Fig. 7. The corresponding boiling curves (water).

perhaps because, again, for $We \leqslant 80$, as also evidenced by Yoshida et al. [2], liquid water droplet rebound phenomena occurs due to the predominant role of water surface tension and the bulk motion of vapor generated from the water droplets. Furthermore, due to a higher latent heat of water, the corresponding boiling curves shown in Figs. 5 and 7 look different in its magnitude. Even though, the present water result is still smaller than that ($q = 4.7 \times 10^5$ W/m^2 at $We = 28$) of Yoshida et al. [2], due to the different subcooling and spray volume flux as well as different heating surface and surface condition, in spite of the same trend found on boiling curves. In fact, also included in Fig. 7 is the data from Yoshida et al. [2] for different test surface. At $\Delta T_{sat} = 30\,^{\circ}$C and $We = 33$, q was found to be about 1.0×10^5 W/m^2 for steady state experiments, which almost has the same value of the present result at $We = 80$. While, for transient results shown in Fig. 7, they are much higher as stated before.

Fig. 8 shows the detailed heat transfer coefficients on the test surface for R-134a at three different Weber numbers at $\Delta T_{sub} = 4\,^{\circ}$C with an average $\bar{h}$ shown for each graph and its corresponding cooling time noted. The results are presented for a circular region over entire surface. The effect of increasing We is clearly seen and is to increase h (or $\bar{h}$). Such phenomena is indicative of a consistency of heat transfer mechanism obtained in Part I and the former discussion (Part II) of this paper which includes boiling curves as well as cooling curves and h–q curves. The photographs for Fig. 8(a)–(c) correspond to a droplet Weber number of 50, 96 and 152 for R-134a.

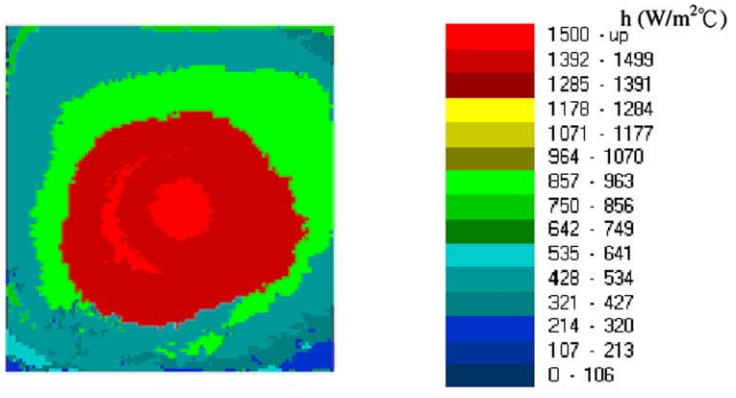

(a) R–134a, We=50

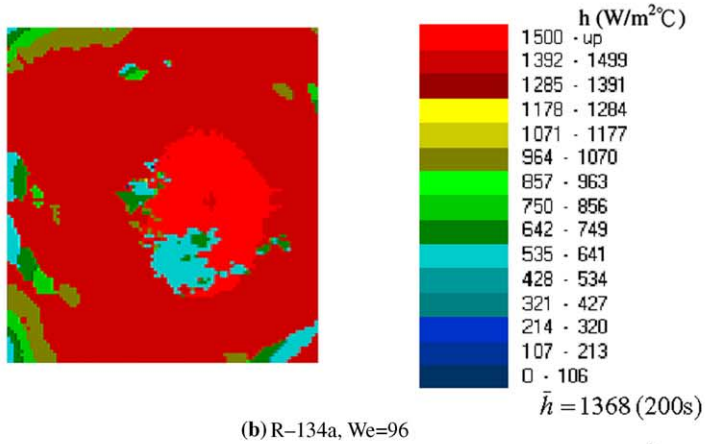

(b) R–134a, We=96

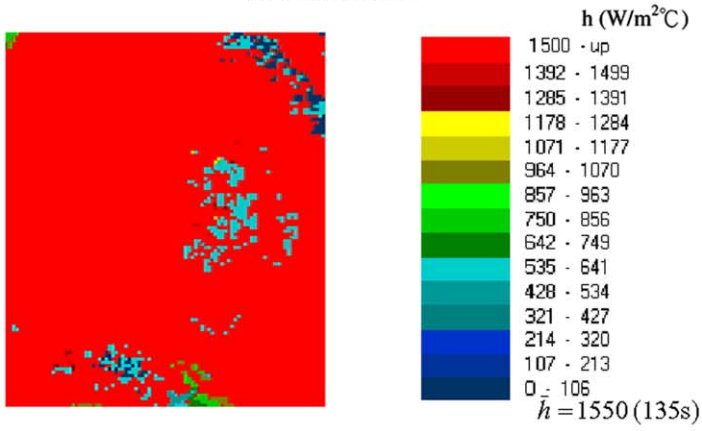

(c) R–134a, We=152

Fig. 8. TLC detailed heat transfer coefficient (ΔT_{sub} = 4 °C).

The droplet impact characteristics at $We = 50$ suggest that relative stable droplets where surface tension forces tend to overcome the breakup effects of inertia and pressure, which results in a relatively low heat transfer as shown in Fig. 8(a). As We increases to 96, it gives the momentum of the droplet, and results in the droplet spreading rate and extent of intact radial film spread to be about 60% greater as shown in Fig. 8(b) with red color than that in Fig. 8(a). At this stage, breakup of the liquid film is caused by liquid ejection and interfacial stabilities due to a plenty of vapor bubble formation as evidenced by Bernardin et al. [4] and Inada and Yang

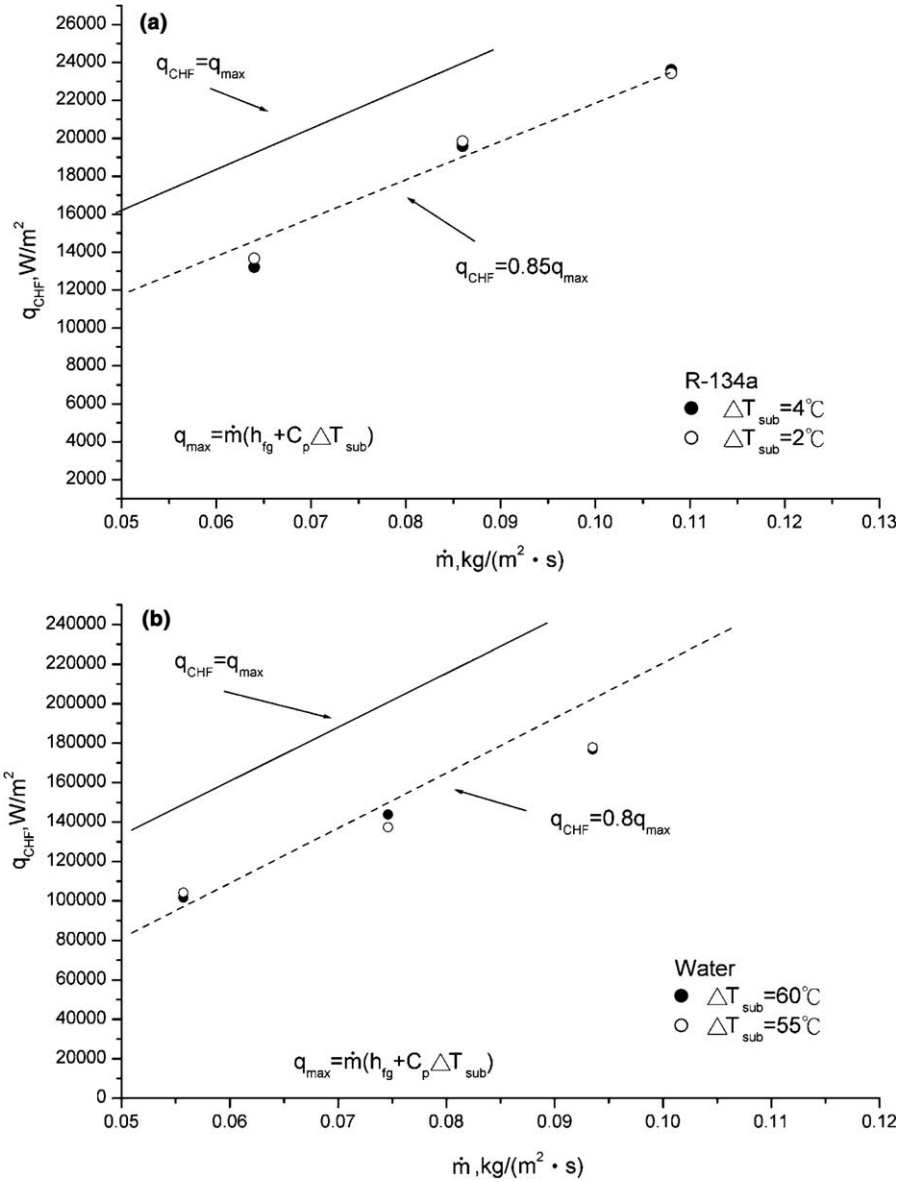

Fig. 9. Relation of CHF and spray volume flux for water and R-134a.

[7]. This behavior would create a series of larger liquid island-like (also globule-like) zones with a fine mist of small droplets mixed as shown in Fig. 8(b). At $We = 152$, excessive boiling and instabilities throughout the entire film were observed and this time the liquid film rapidly breaks up into a lager dispersion of very fine droplets as evidenced by the red color in which a full coverage of the entire region was found (see Fig. 8(c)). These results are very close to those of Kenning and Yan [8] of which a heat transfer coefficient of $1.6\times10^3 \leqslant h \leqslant 2.3\times10^3\,\mathrm{W/m^2\,°C}$ was found for pool boiling heat transfer on a thin plate with liquid crystal thermography. All three Weber number results can be also observed and found in Part I of this paper for boiling visualization and nucleate boiling results.

Finally, the present $q_{max} = q_{CHF}$ and q_{min} results were formulated in terms of the relevant variables. Theoretically, q_{max} can be calculated based on $q_{max} = \dot{m}(h_{fg}+C_p\Delta T_{sub})$ to examine the accuracy of the present measurements. The deviation between q_{CHF} (cooling and boiling curves; e.g. Figs. 4 and 6, 5 and 7) and q_{max} comes from the sources of different kinds of heat losses and all kinds measurement uncertainties. This result is shown in Figs. 9(a) and (b) for R-134a and water,

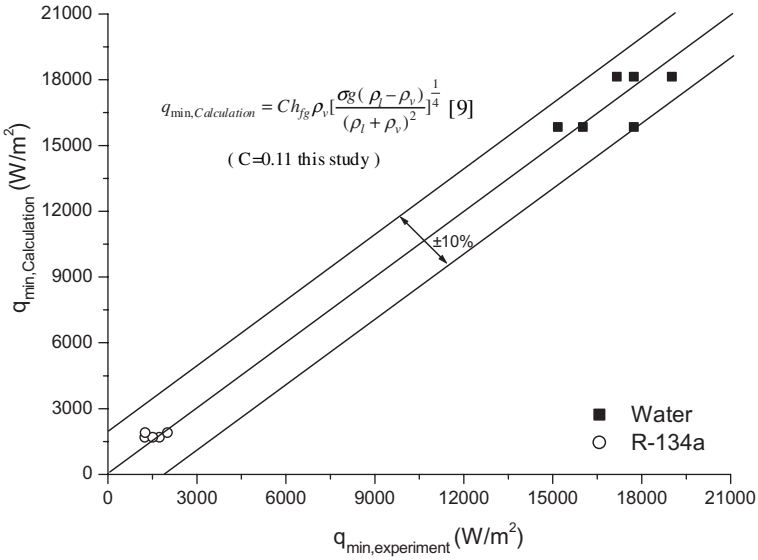

Fig. 10. $q_{min,calculation}$ vs. $q_{min,experiment}$.

respectively. It is found that the present deviation from the theoretical value is about 20%. This strongly suggests that an effective spray cooling was applied for both water and R-134a. Such results are similar to the previous study of Yoshida et al. [2] for water. On the other hand, q_{min} found from experiments (cooling and boiling curves; e.g., Figs. 4 and 6, 5 and 7) was compared with that of empirical correlation, $q_{min} = Ch_{fg}\rho_v(\rho_g(\rho_l - \rho_v)/(\rho_l + \rho_v)^2)^{0.25}$ where $C = 0.09$–0.18 [9] with a $C = 0.11$ found for the present study and the results seem good as the data were located on 45° diagonal line within ±10% band which is shown in Fig. 10.

4. Conclusion

A series of transient experiments which is different from Part I of this paper (steady state) was studied with an aid of TLC technique for liquid sprays of R-134a and water. Both cooling curves as well as the corresponding boiling curves were found. In addition, the MHF and CHF were also measured and compared with those of previous studies [2,9]. Detailed heat transfer distribution on a hot surface was firstly made possible to examine the effect of spray mass flux for R-134a and the data were also extracted to compare with thermocouple measurements. It was found on an average that they two in good agreement within ±10%.

References

[1] K.J. Choi, S.C. Yao, Mechanism of film boiling heat transfer of normally impacting spray, Int. J. Heat Mass Transfer 30 (1987) 311–318.
[2] K. Yoshida, Y. Abe, T. Oka, Y.H. Mori, A. Nagashima, Spray cooling under reduced condition, ASME J. Heat Transfer 123 (2001) 309–318.
[3] Q. Cui, S. Chandra, S. McCahan, The effect of dissolving salts in water sprays used for quenching a hot surface: Part 2—spray cooling, ASME J. Heat Transfer 125 (2003) 333–338.
[4] J.D. Bernardin, C.J. Stebbins, I. Mudawar, Mapping of impact and heat transfer regimes of water drops impinging on a polished surface, Int. J. Heat Mass Transfer 40 (1997) 247–267.
[5] J. Yang, L.C. Chow, M.R. Pais, Nucleate boiling heat transfer in spray cooling, ASME J. Heat Transfer 118 (1996) 668–671.
[6] J.W. Baughn, M.R. Anderson, J.E. Mayhew, J.D. Wolf, Hysteresis of thermochronic liquid crystal temperature measurement based on hue, ASME J. Heat Transfer 121 (1999) 1067–1072.
[7] S. Inada, W.J. Yang, Mechanisms of miniaturization of sessile drops on a heated surface, Int. J. Heat. Mass Transfer 36 (1993) 1505–1515.
[8] D.B.R. Kenning, Y. Yan, Pool boiling heat transfer on a thin plate: features revealed by liquid crystal thermography, Int. J. Heat Mass Transfer 39 (1996) 3117–3137.
[9] Whalley, P.B. Boiling, Condensation and Gas-Liquid Flow, Oxford University Press, Oxford, 1987, p. 201.